Iraqi Geological Journal

Journal homepage: https://www.igj-iraq.org

Paleozoic Back-Arc Basaltic Volcanism in Northern Iraq (Chalki Basalt): Insights into the Geodynamic Evolution of the Paleo-Tethys Ocean

Ahmed M. Aqrawi[1], Alan M. Koyi[2], Nihad M. Karo[1], Jolyana R. Petros[3*]

1 Department of Earth Sciences and Petroleum, College of Science, Salahaddin University, Erbil, Iraq
2 Department of Earth Sciences, Faculty of Science, Vrije University Amsterdam, Amsterdam, Netherlands
3 Department of Geology, College of Science, Duhok University, Duhok, Iraq
* **Correspondence:** e-mail: jolyana.petros@uod.ac

Received:
24 November 2025

Accepted:
16 February 2026

Published:
30 April 2026

Abstract

This study presents petrographic, geochemical, and Sm-Nd isotopic data for the Chalki basaltic rocks (Chalki basalts) from the Zakho area in northern Iraq. These basaltic rocks are intercalated with Pirispiki metasediments and associated with several thrust sheets extending from Bitlis in southeastern Turkey to northern Iraq. Petrography reveals microporphyritic, amygdaloidal textures with primary plagioclase, olivine, and pyroxene, partially altered to zeolite, calcite, and chlorite. Geochemically, the rocks are sub-alkaline tholeiitic basalts with affinities closer to enriched mid-ocean ridge basalt (E-MORB). Trace element patterns, including the absence of a significant negative Eu anomaly, indicate derivation from partial melting of a depleted, spinel lherzolite mantle source within a back-arc basin setting, without substantial plagioclase fractionation. The absence of a negative Eu anomaly suggests minimal plagioclase fractionation. Additionally, the rocks may have formed by partial melting of a depleted mid-oceanic mantle–derived spinel lherzolite in a back-arc basin. Sm-Nd isotopic analysis yields an age of 375 ± 5.5 Ma (Late Devonian, Frasnian), interpreted as the crystallization age. Positive εNd values (+4.8 to +6.2) confirm a depleted mantle origin, though their variation suggests some open-system behavior and minor crustal contamination during ascent. Integrated data indicate that the Chalki basalts represent dismembered fragments of Middle to Late Devonian oceanic lithosphere, subsequently obducted and incorporated into the thrust zone during the closure of the Neo-Tethys Ocean.

Keywords: Northern Iraq; Chalki Basalt; Paleo-Tethys ocean; Sm/Nd dating

1. Introduction

The Chalki basaltic rocks (Chalki basalts), or Chalki Formation, belong to the Paleozoic Era. This formation is part of the Northern Thrust Zone (NTZ), located near the Iraqi-Turkish border. The NTZ is a segment of the extensive Alpine orogeny, represented by the Taurus-Zagros fold-and-thrust belt, which developed as a result of the collision between the Afro-Arabian and Eurasian continents. According to Sharland et al. (2001), the top of the AP4 megasequence (the Paleozoic strata in Iraq comprise five megasequences, AP1 to AP5; Jassim, 2000) is marked by a prominent erosional unconformity, indicated by the presence of Chalki basalts in Iraq. This basaltic volcanism, situated at the northern margin of the Afro-Arabian Plate, is associated with the initiation of northeast-directed subduction beneath the Eurasian Plate (Beydoun, 1991; Sharland et al., 2001).

The Chalki bsalts is intercalated with Pirispiki meta-sediments and associated with several thrust sheets of varying origins and ages. These tectonic slices extend from Bitlis in southeastern Turkey to northern Iraq. The closure of the Neo-Tethys Ocean was marked by the juxtaposition of both allochthonous and autochthonous sequences. These tectonic slices were obducted and stacked to form the Bitlis-Zagros Thrust Zone (BZTZ) (Fig. 1). The BZTZ constitutes the northern segment of the Bitlis-Zagros fold and thrust belt (Bitlis-Zagros FTB), which lies in the northeastern part of the Arabian Plate. In Iraq, this belt forms a narrow zone along the northern border with Turkey, where it is referred to as the NTZ.

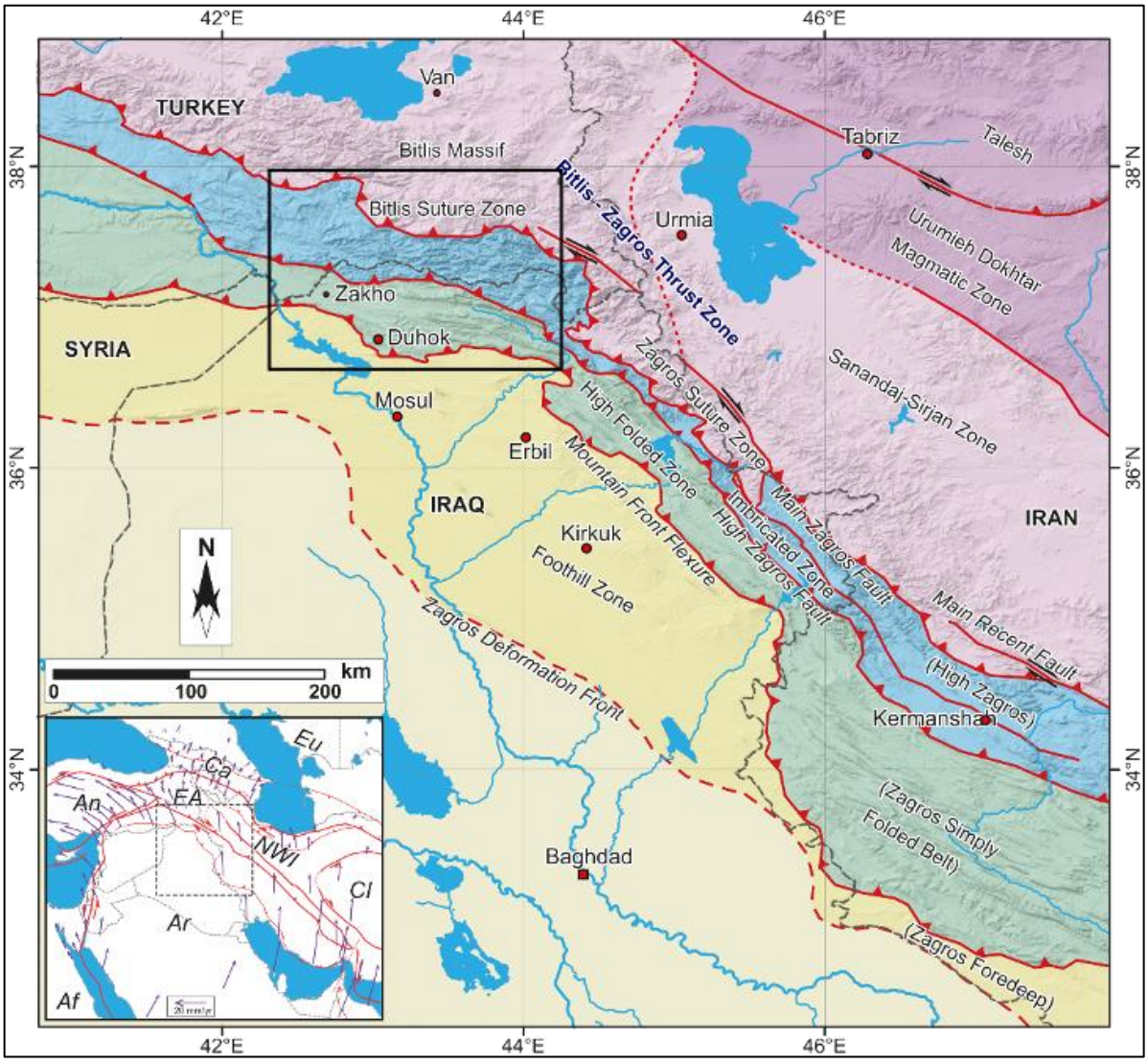


Fig. 1. Tectonic map illustrating the Biltis-Zagros Thrust Zone (modified from Zebari et al., 2020). The black rectangle delineates the area covered in Fig. 2

Together with the Hemrin Basalt (Quaternary) in the Injana Formation within the Low-Folded Tectonic Zone (Kettanah et al., 2021) and the Gercus Basalt (Eocene) in the Gercus Formation within the High-Folded Tectonic Zone (Kettanah and Bamarni, 2018), the Chalki Basalt (Devonian) in the Pirispiki Red Beds within the Imbricate Tectonic Zone can be considered unusual volcanic occurrences not related to the ophiolites that form the Suture Tectonic Zone of NE Iraq. All three of these unusual occurrences are found in sedimentary formations within thick sedimentary sequences as part of prominent anticlinal structures, relatively far from ophiolites and other igneous activities in the region.

Undifferentiated Devonian volcanic rocks found in the Arras Basin in eastern Anatolia, southeastern Turkey, consist of spilite and andesite, accompanied by lithic sandstone (Altinli, 1966). Volcanic rocks have also been identified in the Eastern Taurides of Turkey, which exhibit geochemical characteristics indicative of a back-arc basin environment and are linked to a subduction-related event (Çimen et al., 2016).

The structural characteristics of the NTZ and the specific mechanisms by which thrusting occurred remain relatively poorly understood. Moreover, the region lacks sufficient chronological data to fully reconstruct its tectonic history and establish correlations with the evolution of the Tethys Ocean.

The primary objective of this paper is to clarify the tectonic evolution of the Chalki basalts, with an emphasis on their significance for understanding the evolution of the Tethys Ocean. This interpretation is based on geochemical, petrographic, and geochronological data. In summary, our findings shed light on the paleotectonic evolution along the northeastern margin of Gondwana and provide evidence supporting the reconstruction of paleotectonics within the context of the opening of the Paleo-Tethys Ocean. Van Bellen et al. (1959) assigned an Ordovician age to the studied rocks based on stratigraphic relationships with the surrounding sedimentary sequences. In the present study, radiometric dating ($^{143}Nd/^{144}Nd$ and $^{147}Sm/^{144}Nd$) is applied to directly constrain the age of the Chalki basaltic intrusion.

2. Geological Setting

Chalki basaltic rocks are located about 50 km northeast of Zakho city, near Kaista village, within the Imbricate Tectonic Zone of northern/northeastern Iraq (Figs. 1, 2). Previous studies have concluded that the Chalki basaltic rocks are an integral part of the upper Pirispiki Formation (e.g., Al-Hadidy, 2007; Buday, 1980; Van Bellen et al., 1959). These studies have also considered the basaltic rocks in the Northern Thrust Zone (NTZ) of Iraq, near the Iraqi-Turkish border, as belonging to the Chalki Formation (Ali et al., 2016; Aqrawi et al., 2010; Buday, 1980; Van Bellen et al., 1959). However, the tectonic structure of this group specifically, whether it has been thrust remains poorly understood. Van Bellen et al. (1959) described the lithology of the Chalki Formation as dull green and grayish-green, red-speckled, altered olivine basalt, alternating with intercalations of bright red, ash-bearing, soft siltstone, and shale.

In the study area, the Chalki Formation is interbedded with the Pirispiki Formation. The basaltic rocks consist of altered basaltic flows containing ash. These flows are intercalated with 33 m of red, marly sandstone and silty sandstone; 24 m of quartzite and shale; 16 m of brownish, well-bedded sandstone; and a basal layer comprising 10 m of blocky siltstone.

A regional uplift occurred in the mid-Paleozoic in northern Gondwana and the Arabian Plate, including Iraq (Al-Hadidy, 2007; Ruban et al., 2007). This event led to a significant unconformity at the base of the Upper Devonian in northern Iraq, which is overlain by red beds and basalt. According to Buday (1980), the Pirispiki and Chalki formations should be merged, and the lower section of the Kaista Formation, dating from the Late Devonian to Early Carboniferous, should be reassigned to the Pirispiki Formation. Outcrops of Paleozoic rocks in northern Iraq are visible in the cores of east-west-trending anticlines. Most of these anticlines are asymmetrical: the southern limbs are steeply dipping and strongly deformed by strike-slip faults, whereas the northern limbs dip more gently and are less affected by faulting (Buday and Jassim, 1987; Sissakian and Fouad, 2015).

Sharland et al. (2001) noted that during the Late Devonian to Early Carboniferous, these rocks were deposited in a tectonic setting characterized by both extensional and compressional regimes. This was associated with the so-called “Hercynian event”, which involved back-arc rifting followed by uplift. This interpretation suggests that the Hercynian event on the Arabian Plate may have started earlier than the Late Carboniferous period, as recognized in both North Africa and northern Arabia.

3. Sampling and Methodology

The studied area is located in the northern part of Iraq, in Duhok Province, about 50 km north of Zakho city. Despite the complex geomorphology of the area and its unstable political situation, fieldwork was carried out on an outcrop of Chalki rocks near Kaista village (Fig. 2), at coordinates 36°17′45″N and 43°10′05″E.

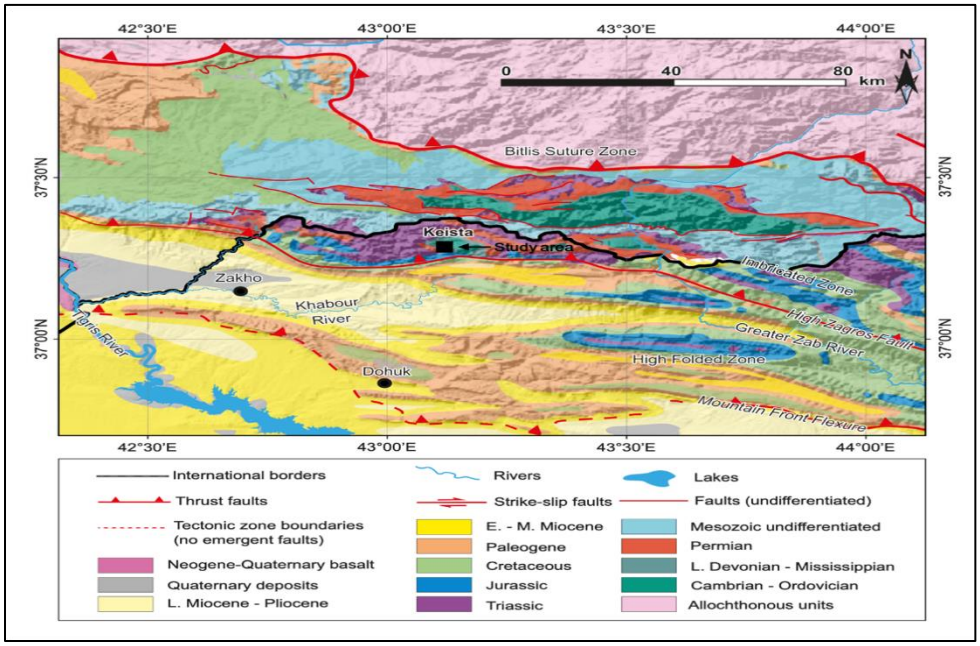


Fig. 2. Geological map showing Chalki Formation and other Paleozoic rocks (Sissakian and Fouad, 2015)

Fifteen rock samples were collected from the Chalki basalts for this study. Thin sections of all samples were prepared for petrographic analysis. Ten of the samples were analyzed for their major and trace-element geochemistry. The samples were analyzed as bulk rocks using a ThermoARL AdvantXP+ automated wavelength-dispersive spectrometer at the GeoAnalytical Laboratory, Washington State University. Major elements were determined using fused glass discs prepared from powdered rock samples, while pressed powder pellets were used for trace-element analysis. Rare earth elements (REEs) were analyzed by inductively coupled plasma mass spectrometry (ICP-MS) after fusing 0.2 g of whole-rock powder with 1.5 g of $LiBO_2$, followed by dissolution in 100 mL of 5% HNO_3.

An accuracy of ±10% is recommended for most elements in the USGS basaltic glass reference materials NIST612 and BCR-2G (e.g., Jochum et al., 2007). Comparison of measured trace element data with the values reported by Jochum et al. (2007) indicates accuracies of +8 to -6 for NIST612 and +7 to -5 for BCR-2G.

Five samples were used for Sm–Nd dating. The Nd and Sm isotope compositions were analyzed using a Thermo Scientific Triton Plus multi-collector thermal ionization mass spectrometer. Isotope measurements were performed at the Laboratory of Geochronological and Environmental Studies at the University of Brasília, Brazil.

For Nd isotope analysis, data were acquired over 10 blocks of 20 cycles, with an integration time of 8 seconds per cycle. Ionization and filament evaporation were initiated gradually, using a heating rate of 5-10 mA/min. To obtain stronger signals (up to 5 V), the heating rate was increased to 50 mA/min, depending on sample composition. Analyses with higher signal intensities and longer acquisition times generally resulted in lower 2σ errors. Target precision for $^{143}Nd/^{144}Nd$ was a 2σ uncertainty of less than

0.000020. Measurements were terminated early if the 2σ value stabilized below ±0.00005 or if the signal became unstable.

For Sm isotopes, data acquisition was set for 10 blocks of 6 cycles with 8 seconds integration time, although measurements usually continued for as long as the sample lasted. Because of smaller signals, the $^{149}Sm/^{152}Sm$ 2σ errors varied between ±0.000010 and ±0.000062, depending on the sample size (~1-75 ng).

An international La Jolla standard was loaded and repeatedly measured using the same method as analyses of the studied samples. The analyses of this international standard yielded a $^{143}Nd/^{144}Nd$ ratio of 0.511827 ± 0.000020 (2σ). Epsilon values were calculated using $^{143}Nd/^{144}Nd_{_CHUR}$ = 0.51264, $^{147}Sm/^{144}Nd_{_CHUR}$ = 0.1967, and $^{147}Sm = 654 \times 10^{-12}$.

4. Results

4.1. Petrography

In the field, the Chalki basalts exhibit dark gray to grayish-brown colors due to extensive oxidation and alteration (Fig. 3). Petrographically, they are classified as spilitic basalts. Petrographic investigation of fifteen Chalki basalt thin sections indicates that the main minerals are olivine, pyroxene, and plagioclase feldspar (Fig. 4). These minerals occur as microphenocrysts within the groundmass of the same minerals and their alteration products (Fig. 4a). Some crystals are up to 1 mm in size, while the groundmass is approximately 0.01 mm. Olivine phenocrysts are relatively larger than other minerals and are distinguished from pyroxene crystals by their clear, vivid colors and lack of cleavage (Fig. 4a, b). Some olivine crystals have been altered (oxidized) to iddingsite (mixed iron oxides and clays) along their borders and fractures, which appear dark brown in color. Feldspars are almost exclusively albitized plagioclase phenocrysts (Fig. 4c, d) with lath-like shapes and polysynthetic twinning (Fig. 4a, c). Lath-shaped plagioclase has been mainly altered to albite, zeolite, and sericite. Pyroxene crystals are mostly subhedral, exhibit cleavage parallel to elongation, and are partially altered to chlorite. The spilitic lavas are commonly amygdaloidal, containing quartz and calcite amygdules. They also exhibit a fine-grained texture, including lath-shaped plagioclase and pyroxene crystals. Titanite and opaque minerals occur as accessory phases. The associated minerals are calcite, sericite, and chlorite. The vesicles in the amygdaloidal textures are filled with quartz, carbonate, and, to a lesser extent, zeolite minerals. The glassy matrix is replaced by chlorite. According to K.C. Dunham, the olivine basalt of Chalki consists of olivine, albitized plagioclase, and their alteration products, such as chlorite, hematite–magnetite pseudomorphs, and ankeritic carbonates (Van Bellen et al., 1959).

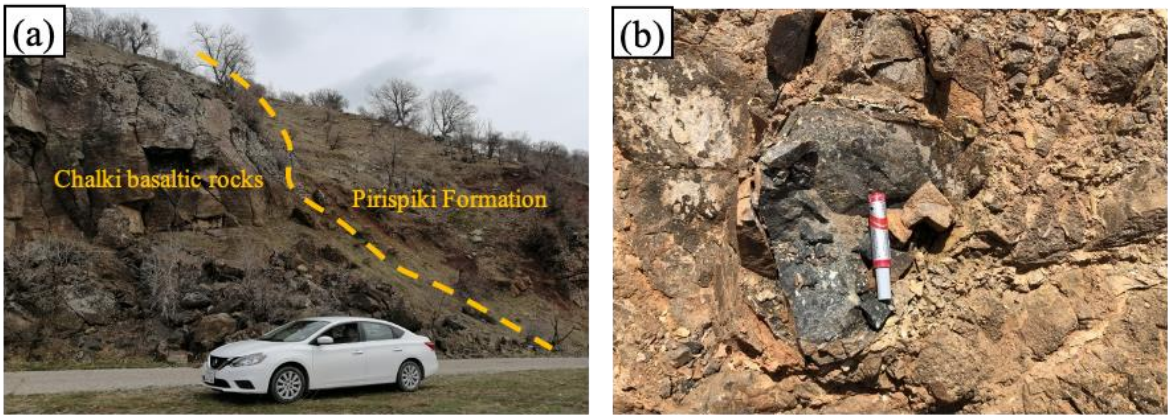


Fig. 3. Field view of the studied basaltic rocks; a) Chalki basaltic rocks is in conformable contact with Pirispiki Formation; b) a close view of Chalki basaltic rocks with amygdaloidal texture

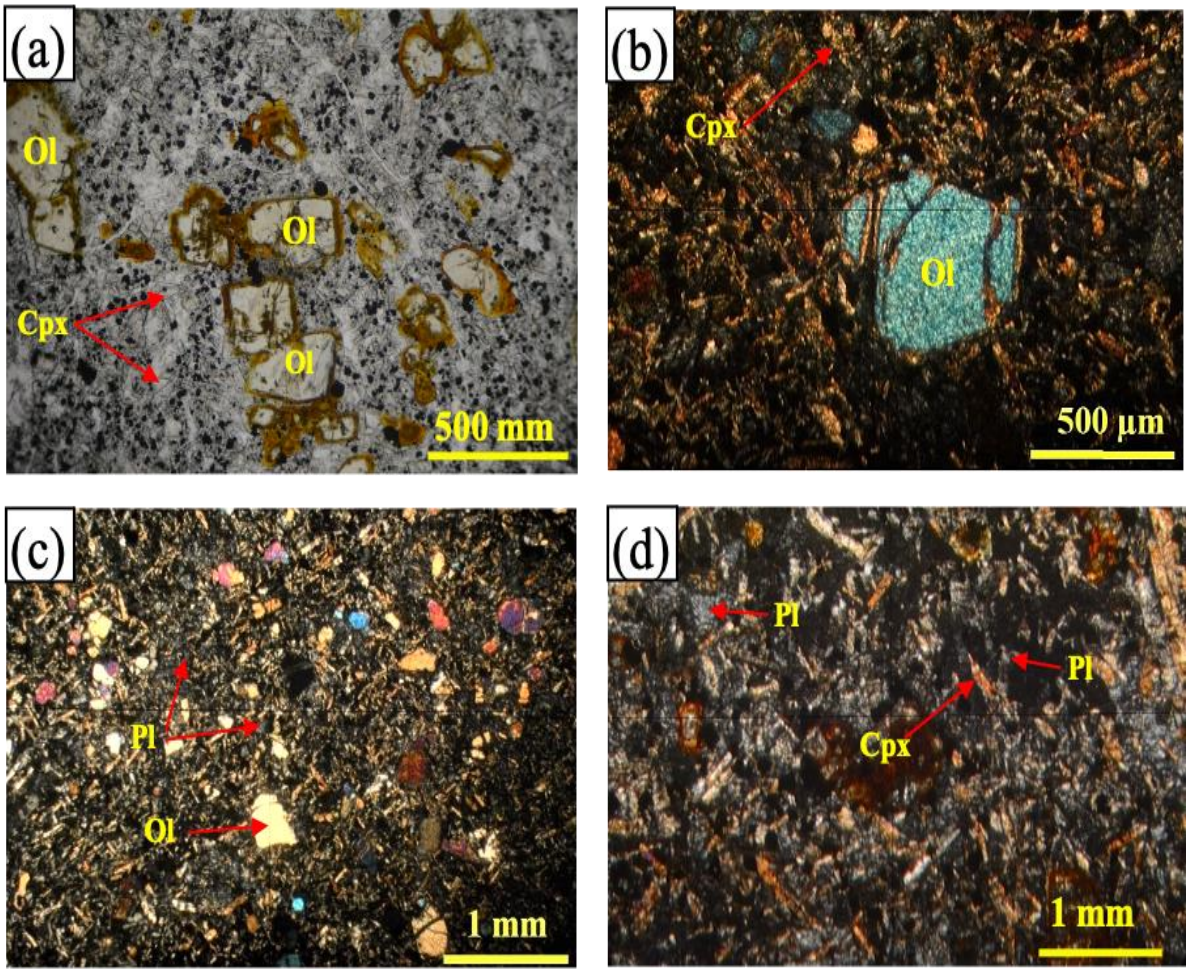


Fig. 4. Photomicrographs of Chalki Basalt showing mineral constituents and textures under transmitted cross-polarized light: a) olivine crystal surrounded by fine pyroxene crystals 10x (XPL) sample S-03; b) Porphyritic texture of olivine, plagioclase and clinopyroxene, 10x, (PPL) sample S-03; c) Olivine phenocrysts surrounded by fine-grained groundmass of pyroxene, plagioclase and ther alteration products, 10x (XPL), sample S-07; d) Fine-grained texture consisting of lath-shaped plagioclase intergrown with elongate pyroxene crystals, 10x, (XPL), sample S-03; Cpx: clinopyroxene, Pl: plagioclase, and Ol: olivine

4.2. Geochemistry

The Chalki basaltic rocks consist of SiO_2 (47.24–54.26 wt%), Al_2O_3 (11.88–17.64 wt%), MgO (1.97–12.84 wt%), FeOt (9.02–15.90 wt%), CaO (0.54–6.45 wt%), and Na_2O (2.53–7.50 wt%) (Table 1). Because the studied rocks have undergone post-crystallization secondary alteration, element mobility in oxides was assessed using Zr as a reference. SiO_2, Al_2O_3, MgO, CaO, Na_2O, and K_2O show no linear relationship with Zr, whereas FeO, TiO_2, and P_2O_5 exhibit clear positive correlations with Zr (Fig. 5). The Mg# values of these rocks vary between 19 and 71. As differentiation progresses, they exhibit increasing enrichment trends in tholeiitic elements such as Ti, Fe, Cr, and Zr (Fig. 6a–d). This study corresponds with that of Ali et al. (2016), who suggested a tholeiitic nature for the Chalki rocks.

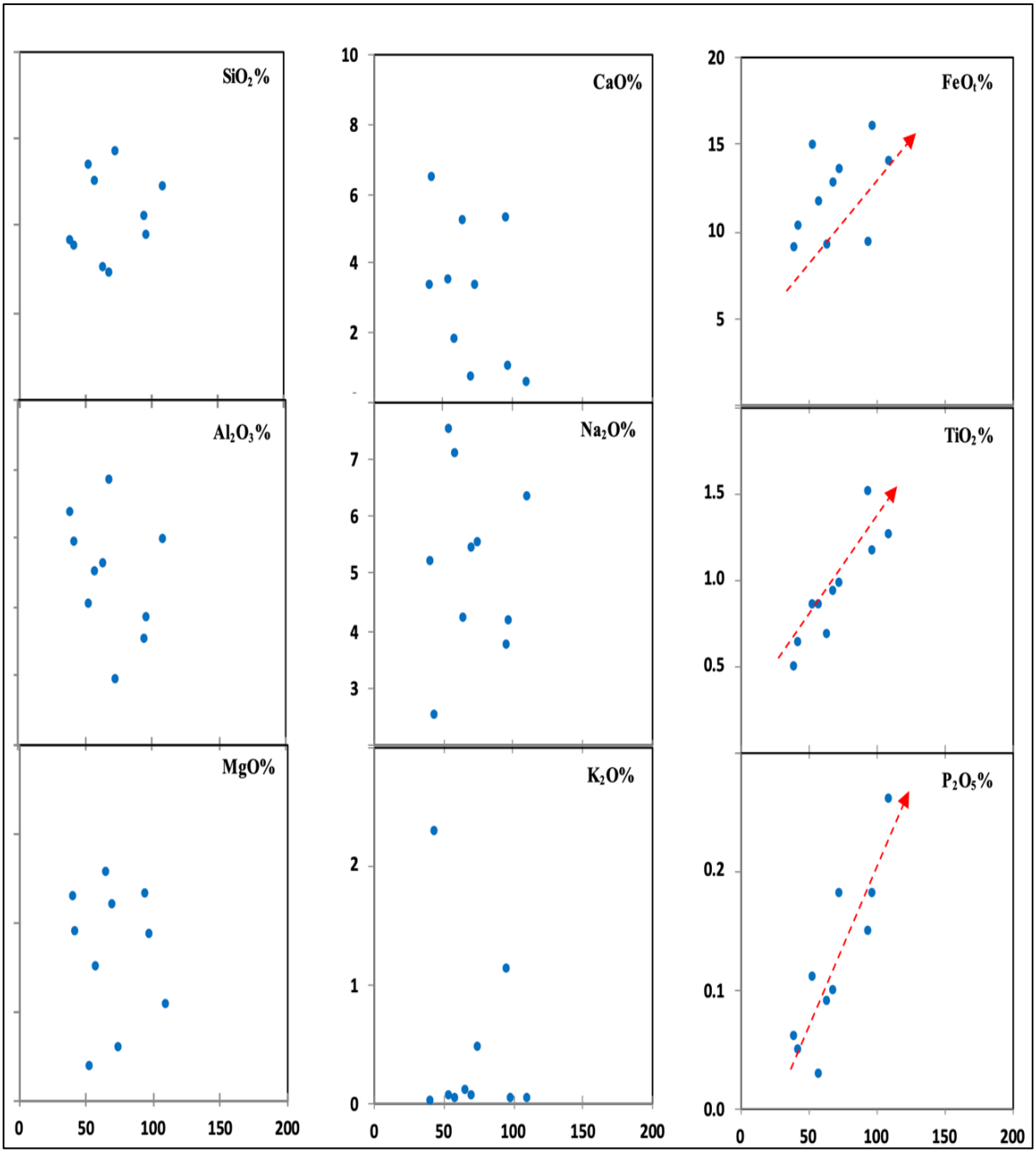


Fig. 5. The effects of element mobility using Zr as a discrimination factor

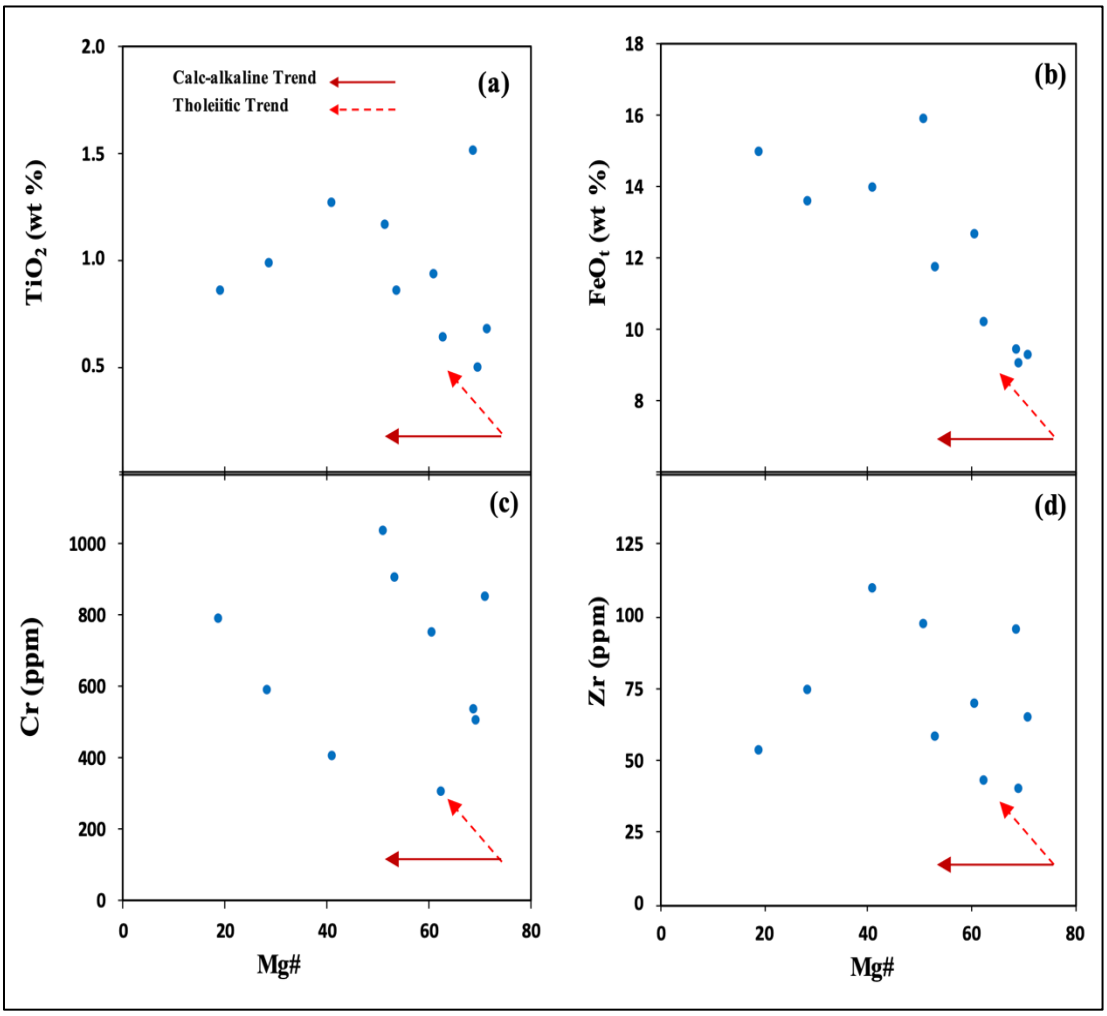


Fig. 6. Diagrams of Mg# (100 × MgO / [MgO + FeO_t] in mole %) versus: a) TiO_2 (wt%); b) total FeO (wt%); c) Cr (ppm); and d) Zr (ppm) for spilitic basalts of the Chalki Formation. The lines indicate calc-alkaline and tholeiitic trends (after Chin et al., 2018).

For the geochemical study of the spilitic basalts from the Chalki Formation, data on major and trace elements were used. Although some of these elements can be mobile during seawater alteration, the paleotectonic setting of the metavolcanics was assessed primarily using immobile elements such as Ti, P_2O_5 (Mullen, 1983), and the lanthanides (Pearce and Norry, 1979). Nonetheless, Si, K, and Na, as well as the alkaline-earth elements (Ca, Sr, Ba), could have undergone varying degrees of redistribution due to the environmental conditions experienced by these rocks. According to Pearce (1983), incompatible large-ion lithophile elements (LILE), such as Cs, Sr, K, Rb, and Ba, exhibit mobility in low-grade metamorphism. Therefore, this study has exclusively focused on elements characterized by their remarkable insolubility in aqueous fluids and their widely accepted immobility during transitions from zeolite to greenschist facies, as outlined by Wood and Graham (1986). These include high-field-strength elements (HFSE), such as Ti, Zr, and Nb (Jiang et al., 2005), rare earth elements (REE) (Sun and McDonough, 1989), and transition elements (Cr, Ni), as well as V (Shervais, 1982). Nonetheless, certain highly altered samples have exhibited notable increases in rare earth elements (especially heavy rare earth elements [HREE]) and thorium (Th), while HFSE have remained largely unaffected (Wharton et al., 1995).

Table 1. Geochemical analyses (major, trace, and REE) of Chalki basaltic rocks

Oxides	S-01	S-02	S-03	S-04	S-05	S-06	S-07	S-08	S-09	S-10	Minimum	Maximum	Mean
Major elements %													
SiO_2	49.39	52.24	53.49	47.59	47.24	49.1	52.48	48.79	54.26	50.49	47.24	54.26	50.51
TiO_2	1.16	1.26	0.85	0.68	0.93	0.49	0.86	0.64	0.98	1.51	0.49	1.51	0.94
Al_2O_3	13.68	15.93	14.06	15.22	17.64	16.76	15.02	15.89	11.88	13.05	11.88	17.64	14.91
Cr_2O_3	0.106	0.045	0.075	0.086	0.075	0.05	0.09	0.028	0.057	0.055	0.028	0.106	0.07
FeOt	15.9	13.94	14.96	9.24	12.68	9.02	11.7	10.21	13.54	9.4	9.02	15.9	12.06
MnO	0.19	0.05	0.18	0.37	0.15	0.47	0.15	0.13	0.12	0.11	0.05	0.47	0.19
MgO	9.36	5.45	1.97	12.84	10.99	11.51	7.52	9.56	3.02	11.64	1.97	12.84	8.39
CaO	1.05	0.54	3.48	5.21	0.74	3.35	1.82	6.45	3.32	5.27	0.54	6.45	3.12
Na_2O	4.19	6.35	7.5	4.24	5.44	5.23	7.08	2.53	5.55	3.76	2.53	7.5	5.19
K_2O	0.05	0.04	0.06	0.1	0.07	0.02	0.04	2.28	0.47	1.13	0.02	2.28	0.43
P_2O_5	0.18	0.26	0.11	0.09	0.1	0.06	0.03	0.05	0.18	0.15	0.03	0.26	0.12
LOI	4.6	3.8	3.4	4.1	4.2	3.7	3.1	3.5	4.8	3.8	3.1	4.8	3.90
Total	99.88	99.91	100.1	99.77	96.06	99.76	99.89	100.1	98.18	100.4	96.06	100.37	99.40
Trace elements (ppm)													
Ba	215	117	109	60	223	198	265	453	144	262	60	453	204.60
Sc	38	36	44	37	48	41	40	43	25	19	19	48	37.10
Co	44.8	36.2	15.7	61.1	73.5	44.6	52.2	56.1	22.9	52.4	15.7	73.5	45.95
Zn	342	152	27	384	138	765	110	46	36	110	27	765	211.00
Ni	180	116	115	221	227	152	196	114	126	215	114	227	166.20
Hf	2.4	2.7	1.6	2.1	2.1	1.2	1.5	1.6	2.1	2	1.2	2.7	1.93
Nb	13.2	9.3	3.1	3.7	4.6	1.7	3.3	1.6	5.1	10.4	1.6	13.2	5.60
Rb	1.1	1.2	1.5	2.1	1.1	0.6	0.5	10.7	23.1	18.6	0.5	23.1	6.05
Sr	64.3	51.4	77.2	152.1	77.3	144.7	80.6	114.5	49.6	213.9	49.6	213.9	102.56
Ta	0.4	0.6	0.1	0.2	0.1	0.1	0.2	0.1	0.3	0.5	0.1	0.6	0.26
Th	2.4	1.7	1.3	0.4	1.5	0.5	0.7	0.3	0.9	2.2	0.3	2.4	1.19
U	1.1	2.1	0.2	0.1	0.4	0.2	0.1	0.2	0.3	0.6	0.1	2.1	0.53
V	274	243	192	242	319	190	78	290	170	168	78	319	216.60
Zr	97.1	109.5	53.2	64.5	69.4	39.8	57.7	42.6	73.5	94.6	39.8	109.5	70.19
Y	25.2	23.3	17.3	19.6	25.5	17.3	19.8	21.4	18.2	20.3	17.3	25.5	20.79
REE (ppm)													
La	5.8	6.2	3.5	4.1	6.2	2.3	5.4	2.4	2.3	12.7	2.3	12.7	5.09
Ce	12.2	12.8	6.4	9.6	8.9	5.4	10.5	6.1	4.3	26.6	4.3	26.6	10.28
Pr	2.14	1.65	0.91	1.38	1.38	0.83	1.58	0.97	0.64	3.46	0.64	3.46	1.49
Nd	10.1	6.7	4.3	6.1	7.5	4.2	6.4	5.3	2.8	15.1	2.8	15.1	6.85
Sm	3.41	2.42	1.3	2.1	2.4	1.43	1.9	2.11	1.2	4.22	1.2	4.22	2.25
Eu	1.24	0.83	0.46	0.79	0.94	0.74	0.73	0.82	0.53	1.62	0.46	1.62	0.87
Gd	3.86	3.21	1.92	2.77	3.58	2.11	2.68	2.78	2.15	4.58	1.92	4.58	2.96
Tb	0.7	0.62	0.41	0.5	0.58	0.43	0.47	0.51	0.42	0.73	0.41	0.73	0.54
Dy	4.48	4.02	2.91	3.4	3.82	3.04	3.26	3.58	2.95	4.31	2.91	4.48	3.58
Ho	0.9	0.92	0.64	0.79	0.88	0.63	0.71	0.75	0.63	0.76	0.63	0.92	0.76
Er	2.87	2.86	2.08	2.53	2.81	1.9	2.43	2.51	2.06	1.96	1.9	2.87	2.40
Tm	0.36	0.41	0.32	0.35	0.38	0.29	0.32	0.35	0.31	0.26	0.26	0.41	0.34
Yb	2.5	2.87	2.01	2.44	2.76	1.97	2.25	2.28	2.04	1.6	1.6	2.87	2.27
Lu	0.4	0.48	0.37	0.38	0.45	0.32	0.31	0.34	0.33	0.24	0.24	0.48	0.36
Mg#	51.21	41.07	19.01	71.24	60.71	69.47	53.40	62.54	28.45	68.83	19.01	71.24	52.59
Zr/Y	3.85	4.70	3.08	3.29	2.72	2.30	2.91	1.99	4.04	4.66	2.30	4.29	3.38
Zr/TiO_2	0.008	0.009	0.006	0.009	0.007	0.008	0.007	0.007	0.008	0.006	0.008	0.007	0.007
Th/Ta	6.00	2.83	13.00	2.00	15.00	5.00	3.50	3.00	3.00	4.40	3.00	4.00	4.58
Th/Yb	0.96	0.59	0.65	0.16	0.54	0.25	0.31	0.13	0.44	1.38	0.19	0.84	0.52
Ta/Yb	0.16	0.21	0.05	0.08	0.04	0.05	0.09	0.04	0.15	0.31	0.06	0.21	0.11
(La/Sm)n	1.10	1.66	1.75	1.27	1.68	1.04	1.85	0.74	1.25	1.95	1.25	5.00	3.29
(Gd/Yb)n	1.29	0.93	0.80	0.95	1.08	0.89	0.99	1.02	0.88	2.39	0.01	0.03	0.01
(La/Yb)n	2.41	2.24	1.81	1.74	2.33	1.21	2.49	1.09	1.17	8.24	1.17	8.24	2.47
Eu/Eu*	1.02	0.89	0.87	0.98	0.96	1.27	0.97	1.01	0.99	1.10	33.90	74.29	64.16

n: Chondrite normalized (McDonough and Sun, 1995).

Eu/Eu*: Eu anomaly which was calculated according to $[Eu_n/\sqrt{(Sm_n)\ (Gd_n)}]$

The chemical variation diagrams (Nb/Y vs. Zr/TiO_2 and P_2O_5 vs. Zr) (Winchester and Floyd, 1977) show that the Chalki basaltic samples fall within the sub-alkaline basalt field (Fig. 7a and b). The Chalki basalts are characterized by relatively higher ratios of Zr/Y (3.35), Th/Ta (5.77), Th/Yb (0.54), and Ta/Yb (0.12) compared to typical mid-ocean ridge basalts (2.64, 0.75, 0.04, and 0.043, respectively) (Sun and McDonough, 1989). These geochemical signatures are indicative of subduction-related basalts, back-arc basin basalts, and enriched mid-ocean ridge basalts (Sun and McDonough, 1989).

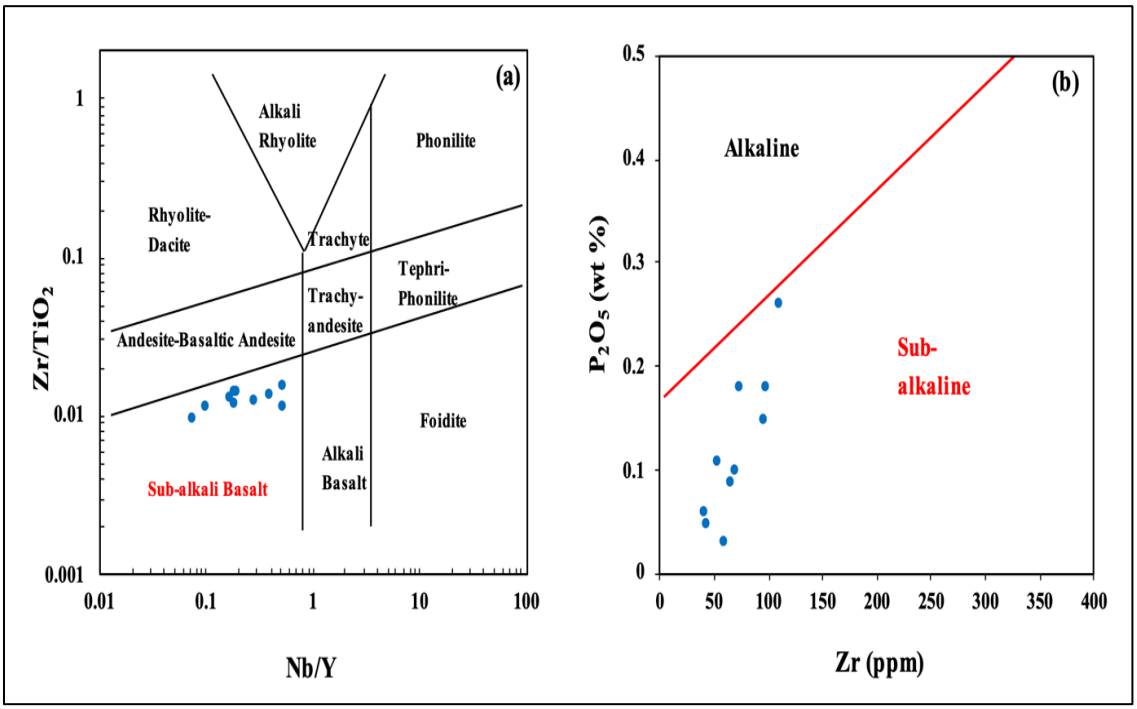


Fig. 7. a) Nb/Y vs. Zr/TiO_2 (ppm) diagram for the classification of spilitic basalts from the Chalki Formation (after Winchester & Floyd, 1977); b) Zr vs. P_2O_5 variation diagram used to discriminate between precursors of alkali basalt and tholeiitic affinity (after Sun and McDonough, 1989)

The normalized N-MORB and chondrite (Sun and McDonough, 1989) trace and rare earth element spider diagrams of the spilitic lavas in this study reveal a closer resemblance to enriched mid-ocean ridge basalts (E-MORB) rather than N-MORB and ocean island basalts (OIB), as described by Sun and McDonough (1989) (Fig. 8a and b). The spilitic basalts exhibit a relatively horizontal trend or a depletion in LREE relative to HREE, and a few show enrichment in LREE relative to HREE (LREE; La = 22× chondrite) while displaying a horizontal trend in middle and heavy rare earth elements (MREE and HREE; Lu = 14× chondrite).

Additionally, these rocks show enrichment in large-ion lithophile elements (LILE), such as Rb, Ba, and Th, and depletion in high-field-strength elements (HFSE), such as Zr, Hf, and Ti. Negative anomalies in Nb and Ti relative to La and Ce are indicative of geochemical features associated with subduction processes. The absence of a negative Eu anomaly (Eu/Eu* = 0.89-1.30), where Eu/Eu* = $(Eu)N/[(SmN \times GdN)^{0.5}]$ (Taylor and McLennan, 1995), suggests that plagioclase fractionation was not significant during magmatic processes (Woodhead, 1988). The average normalized (La/Yb)N, (La/Sm)N, and (Gd/Yb)N ratios is 2.47, 3.29, and 0.01, respectively. These values resemble E-MORB (1.80, 1.53, and 1.02) more than N-MORB.

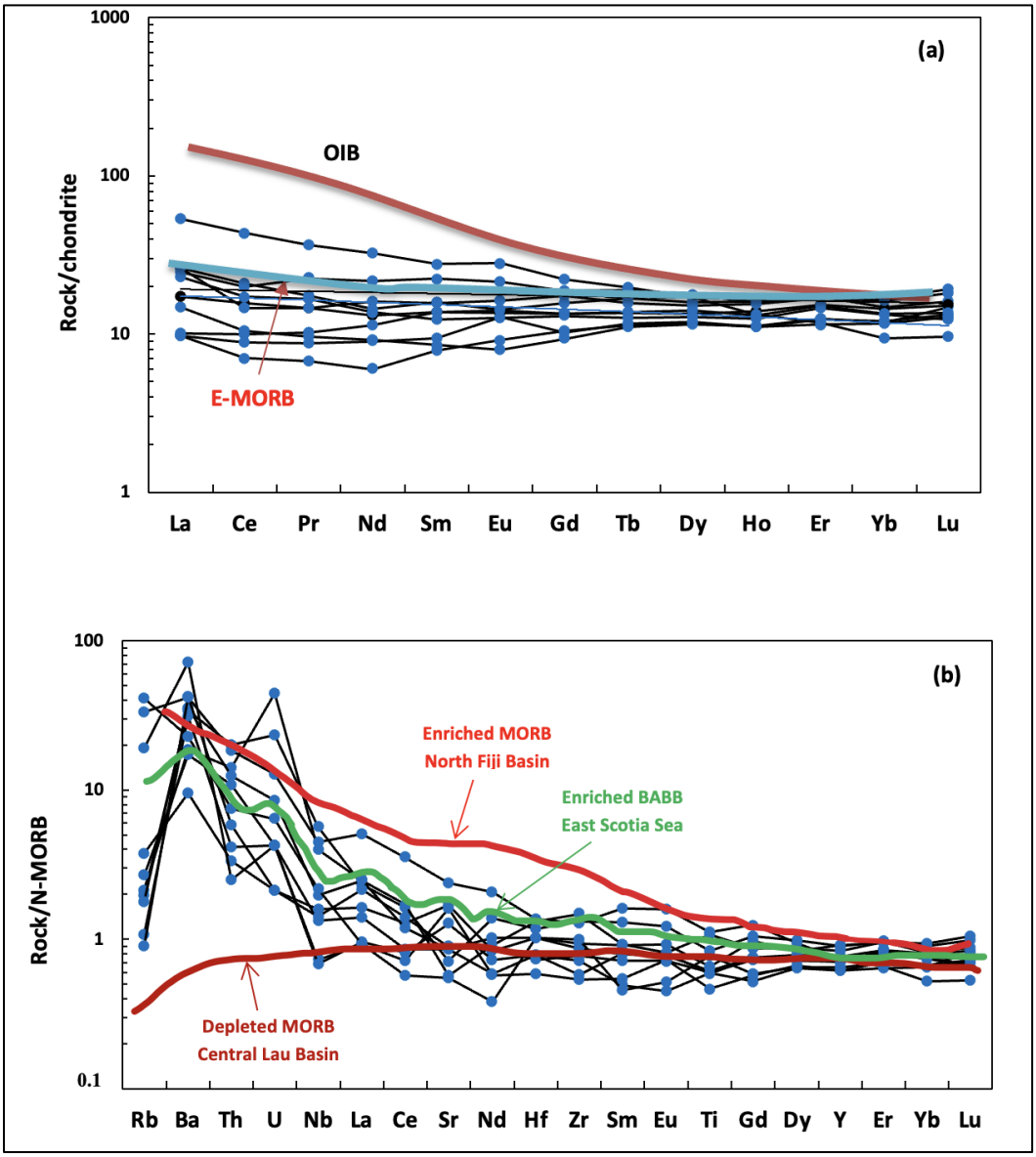


Fig. 8. a) Rare Earth Element (REE) diagram normalized to chondrite values; b) Trace element spider diagram normalized to N-MORB values (normalization data for both diagrams are based on Sun and McDonough, 1989). Data for enriched and depleted MORB, as well as enriched back-arc basin basalt (BABB), are sourced from Pearce and Stern (2006)

4.3. Sm-Nd isotopes

Five samples of Chalki Basalt were analyzed for Sm/Nd whole-rock isotopes. The analytical results are listed in Table 2 and show moderate Sm and Nd concentrations (1.82-4.016 ppm Sm, 4.512-13.958 ppm Nd) relative to NMORB. The measured $^{143}Nd/^{144}Nd$ ratios exhibit slight variation, ranging from 0.5127 to 0.5132, and all samples yielded acceptable analytical results reported in Table 2. This table also presents the calculated isochron ages alongside epsilon notation (εNd) values, which are used to interpret and present the neodymium isotopic data. The analyzed samples display limited variation in their Nd isotope compositions, with εNd values ranging from +4.8 to +6.2, as detailed in Table 2.

Isochron plots of the Chalki Basalt are shown in Fig. 9a. The calculated age for these rocks is 375 ± 5.5 Ma. The variation in εNd values (+4.8 to +6.2, Table 2) suggests that the isotopic system was not completely closed and that these basaltic magmas experienced some contamination with crustal

materials during ascent (Whalen et al., 1999). The positive εNd values indicate a depleted-mantle source (Jacobsen and Wasserburg, 1984; Fig. 9b). Conversely, the elevated $^{143}Nd/^{144}Nd$ ratios observed in all samples likely represent typical values for mid-ocean ridge basalts (e.g., Gale et al., 2013), suggesting that the mantle source underwent significant crust-mantle interaction (Jacobsen and Wasserburg, 1984).

Table 2. Sm-Nd data of spilitic basalts from Chalki Formation

Sample No.	NGR	Sm ppm	Nd ppm	$^{147}Sm/^{144}Nd$	$^{143}Nd/^{144}Nd$	epsilon Nd	Age (Ma)
S-01	SX7383-3800	2.823	8.611	0.1359	0.5128	+5.5	380
S-04	SX7383-3998	1.820	6.214	0.2350	0.5132	+6.2	375
S-05	SX6677-5403	2.319	8.176	0.1365	0.5127	+4.8	380
S-08	SX6643-5380	2.414	4.512	0.2420	0.5132	+6.1	375
S-10	SX6643-5380	4.016	13.958	0.1336	0.5127	+4.9	375

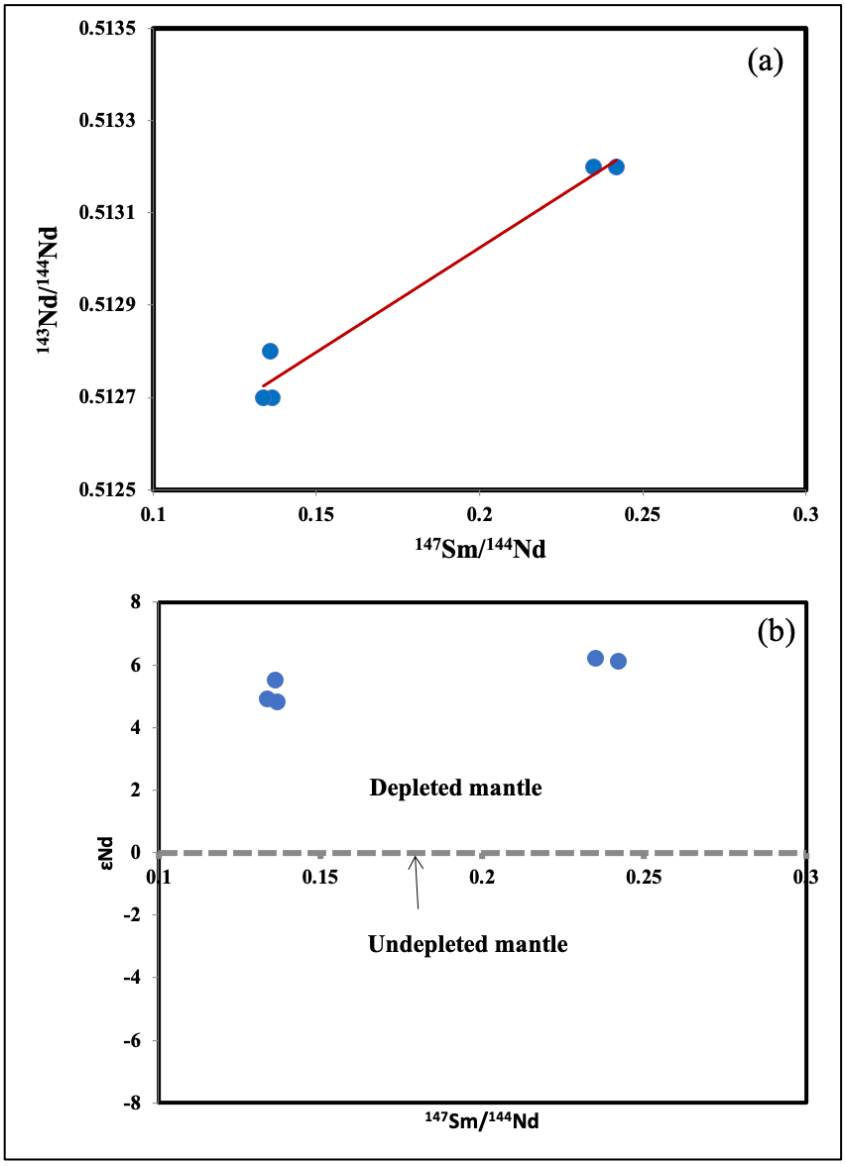


Fig. 9. Isotopic data of Chalki basaltic rocks plotted on the Sm-Nd evolution diagram (adapted from Jacobsen & Wasserburg, 1984): a) $^{143}Nd/^{144}Nd$ versus $^{147}Sm/^{144}Nd$ (initial $^{143}Nd/^{144}Nd$ = 0.51271); b) Epsilon notation (εNd) versus $^{147}Sm/^{144}Nd$

5. Discussion

5.1. Petrogenesis

The influence of magmatic differentiation on the studied rocks is reflected in the negative correlation observed in the TiO_2 versus Al_2O_3/TiO_2 plot (Fig. 10a; Arndt et al., 2008). The spilitic basalts from the Chalki basaltic suite exhibit elevated Cr_2O_3 levels (0.106–0.28 wt%) relative to basalts derived from mantle-source primary magma (~300 ppm) and moderately high Ni concentrations (114–227 ppm). Th/Nb ratios of 0.11–0.42 in these basalts suggest a slight enrichment compared to typical MORB (0.04–0.07) and OIB (0.08) values, as reported by Sun and McDonough (1989). The Ti/Y ratios of 195–416 are generally lower than those of N-MORB (272) and OIB (593) (Sun and McDonough, 1989).

Furthermore, the Ti/Zr versus V/Ti diagram (Fig. 10b) implies that partial melting of N-MORB, in the range of 1–20%, is required to generate the Chalki basaltic rocks. Evidence from the Y-Cr variation diagram of Floyd et al. (1991) supports significant fractional crystallization involving clinopyroxene and plagioclase, indicating that these rocks may have originated from 5–30% partial melting of a spinel lherzolite source (Fig. 10c and d). In addition, the Zr/Nb versus La/Y diagram suggests that these rocks likely derived from partial melting of a spinel lherzolite mantle source, rather than from a garnet lherzolite source typical of the depleted mid-ocean mantle (DMM) (Fig. 10d).

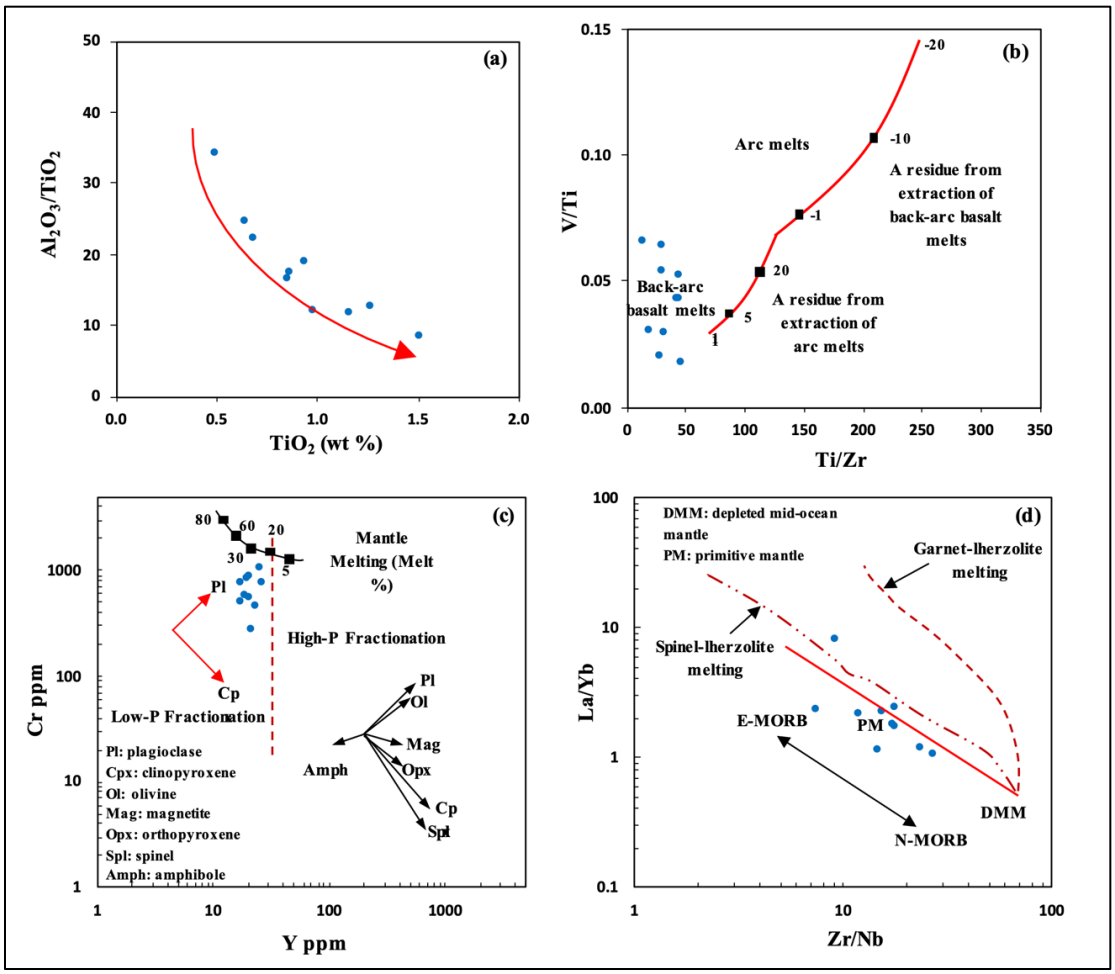


Fig. 10. a) TiO_2 vs. Al_2O_3/TiO_2 diagram illustrating the effects of magmatic differentiation in the spilitic basalts; b) Ti/Zr vs. V/Ti diagram (after Shervais, 1982) showing melt and residue compositions resulting from ~1-20% partial melting of a typical N-MORB source. The plotted samples fall within the compositional field of back-arc basalt melts; c) Y vs. Cr diagram (Floyd et al., 1991), indicating batch melting trends from a spinel lherzolite source, consistent with the geochemical behavior of the studied

rocks; d) Zr/Nb vs. La/Yb diagram (modified after Aldanmaz et al., 2000), suggesting that the metavolcanic rocks originated from partial melting of a spinel-bearing lherzolite mantle source, rather than a garnet-bearing lherzolite derived from a depleted mantle reservoir

5.2. Tectonic discrimination

Subduction-related magmas are typically characterized by enrichment in large-ion lithophile elements (LILE) relative to high-field-strength elements (HFSE). The spider diagram patterns of the most samples reveal enrichment in Nb and depletion in Ti, along with modest enrichment in light rare earth elements (LREE) compared to heavy rare earth elements (HREE), with normalized $(La/Yb)_n$ ratios ranging from 0.72–5.39 and $(La/Sm)_n$ and $(Gd/Yb)_n$ ratios between 1.0–1.88 (Fig. 8a, b). Such enrichment in LREE relative to low Nb concentrations is commonly interpreted as a signature of subduction-related magmatism (Sun and McDonough, 1989). Therefore, the geochemical characteristics of the analyzed samples point to a subduction-related origin rather than derivation from a normal mid-ocean ridge basalt (N-MORB) source.

In contrast to MORB, volcanic arc basalts, and back-arc basin basalts, within-plate basalts typically exhibit higher Ti/Y and Nb/Y ratios (Rollinson, 1993). When plotted on the Ti/Y vs. Zr/Y diagram of Pearce and Gale (1977), the studied rocks fall within the plate-margin basalt field, indicating relative enrichment in Zr and Ti compared to within-plate basalts (Fig. 11a). Additionally, in the Zr vs. Ti/Zr diagram of Akhtar et al. (2021), the spilitic basalts from this study lie within the compositional range of back-arc basin basalts (Fig. 11b).

The Y vs. La/Nb diagram is a useful tool for distinguishing between MORB, back-arc basin basalts (BABB), and island arc tholeiites (IAT), as proposed by Floyd et al. (1991; Fig. 11c). In general, arc tholeiites exhibit La/Nb ratios greater than 5, often exceeding 10, reflecting a mature arc setting. In contrast, alkali basalts, typically influenced by within-plate mantle sources, display lower La/Nb ratios, ranging from 1–5 (Brown et al., 1984). The spilitic basalts from the studied area show low Y and La/Nb ratios, a characteristic feature of BABB, as illustrated in Fig. 11c.

Furthermore, the Chalki Basalt is characterized by low V/Ti ratios (0.017–0.065), which are lower than those typically observed in IAT. These basalts also exhibit slightly reduced Zr values compared to N-MORB. When plotted on the Zr vs. V/Ti diagram of Woodhead et al. (1993), sample compositions span the BABB, IAT, and MORB fields, indicating transitional geochemical affinities (Fig. 11d). However, when integrated with earlier tectonic discrimination plots in Figures 11b and 11c, the data are most consistently interpreted as representing a BABB setting. Despite their overall back-arc geochemical signature, the major and trace-element compositions of the basaltic magmas suggest that they experienced some degree of crustal contamination during ascent. This is evidenced by relatively high Na_2O contents, reaching up to 7.5 wt% (Table 1), likely resulting from spilitization. Additionally, the trace-element patterns display a pronounced negative Nb anomaly (Fig. 8b), further supporting the influence of crustal material.

The geochemistry of immobile trace elements indicates that the studied basalts exhibit typical features of back-arc basin basalts (BABBs). BABBs are characterized by broad compositional diversity, encompassing signatures similar to N-MORB, E-MORB, island arc basalts (IAB), and ocean island tholeiites (OIT), reflecting substantial heterogeneity in their mantle source. Taking into account the combined geochemical and geochronological evidence, the Chalki Basalt is interpreted as an allochthonous fragment derived from the Middle to Late Devonian oceanic lithosphere.

This study, conducted on the northeastern Arabian Plate, presents findings from the Chalki basaltic unit that confirm a mid-ocean ridge basalt (MORB) age of 375 million years, determined through Sm-Nd analysis. This age aligns with the maximum depositional age of 334 ± 12.5 million years for the upper Pirispiki Formation (Koshnaw et al., 2021), based on sample 14KRD-371, which is stratigraphically positioned above the Chalki volcanic unit (Koshnaw et al., 2017). Additionally, the

results of the studied rocks correspond with a juvenile xenolith crustal sample from southern Syria, dated at 357 million years (Stern et al., 2014), as well as with a significant thermotectonic cooling event documented from the Late Devonian to Early Carboniferous periods. This event, dated at approximately 373 ± 26 million years, is based on zircon fission-track data from the Magrish migmatite in the northwestern Arabian Shield (sample Y-135J; Kohn et al., 1992).

Sharland et al. (2001) described the tectonism in Arabia during the Late Devonian to Early Carboniferous as related to the Hercynian orogeny. However, the spatial extent of this deformation remains poorly understood, and its impact on northeastern Arabia is still unclear. Alternatively, the timing of Chalki volcanism aligns with the opening of either the Proto-Tethys (Cambrian to Devonian) or the Paleo-Tethys (mid-Silurian to Mesozoic) oceans (Fig. 7; Ruban et al., 2007). Given the Paleo-Tethys mid-ocean ridge's proximity to northeastern Arabia, it is more plausible that Chalki volcanism is associated with the opening of the Paleo-Tethys. Overall, the Chalki basalt results provide new insights into the paleotectonic evolution of the northeastern Gondwanan margin and contribute to detailed paleotectonic reconstructions related to the Paleo-Tethys realm.

Pearce and Stern (2006) used Nb/Yb ratios as tracers to monitor mantle flow, revealing that mantle flow in arc-basin systems varies due to factors such as subduction-driven corner flow, flow around subduction edges, and the presence of flow barriers. They also employed Ba/Nb ratios as indicators of subduction input, demonstrating that the extent of this input depends largely on basin evolution, mantle-flow patterns, and the proximity of volcanic arcs. The Nb/Yb and Ba/Nb ratios were applied to the studied samples, as illustrated in Fig. 12a.

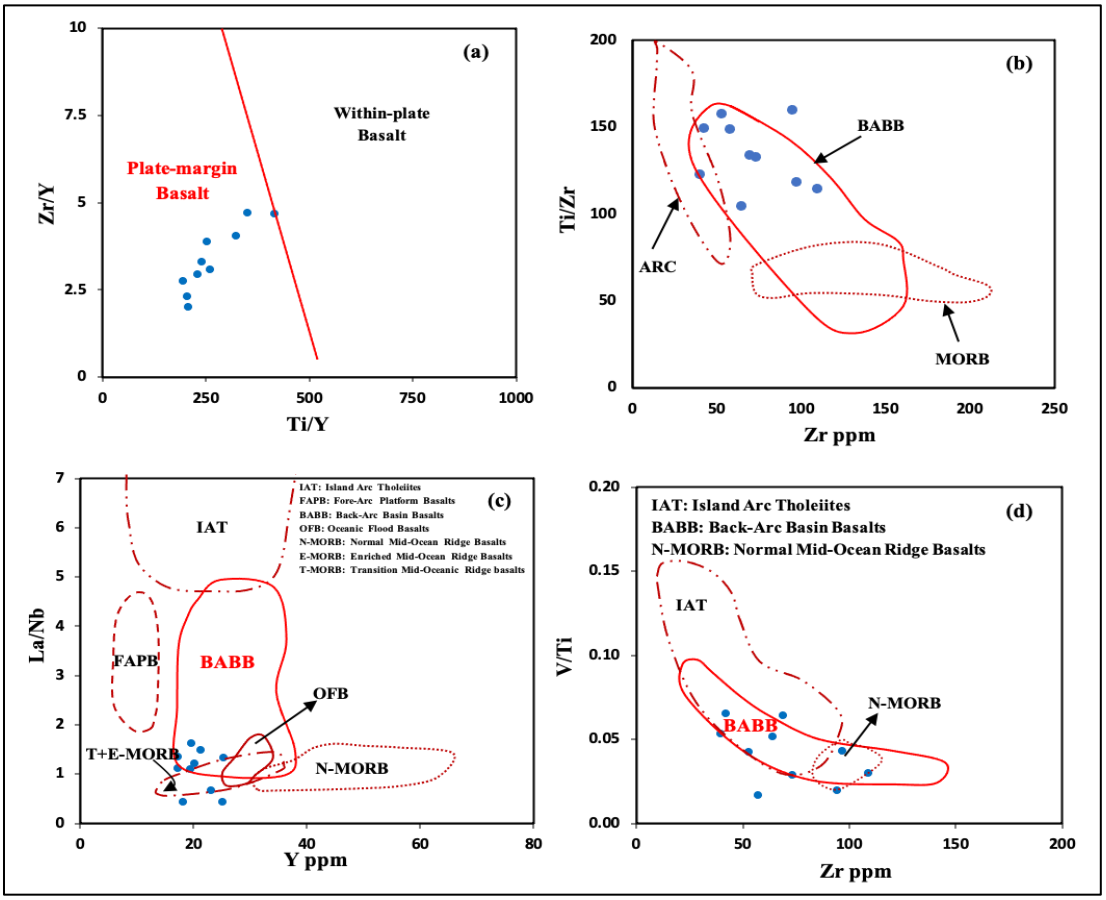


Fig. 11. Tectonic discrimination diagrams for spilitic basalts from the Chalky formation: a) Ti/Y versus Zr/Y (adapted from Pearce and Gale, 1977); b) Zr versus Ti/Zr (modified after Akhtar et al., 2021); c) Y versus La/Nb (based on Floyd et al., 1991); (d) Zr versus V/Ti (from Woodhead et al., 1993

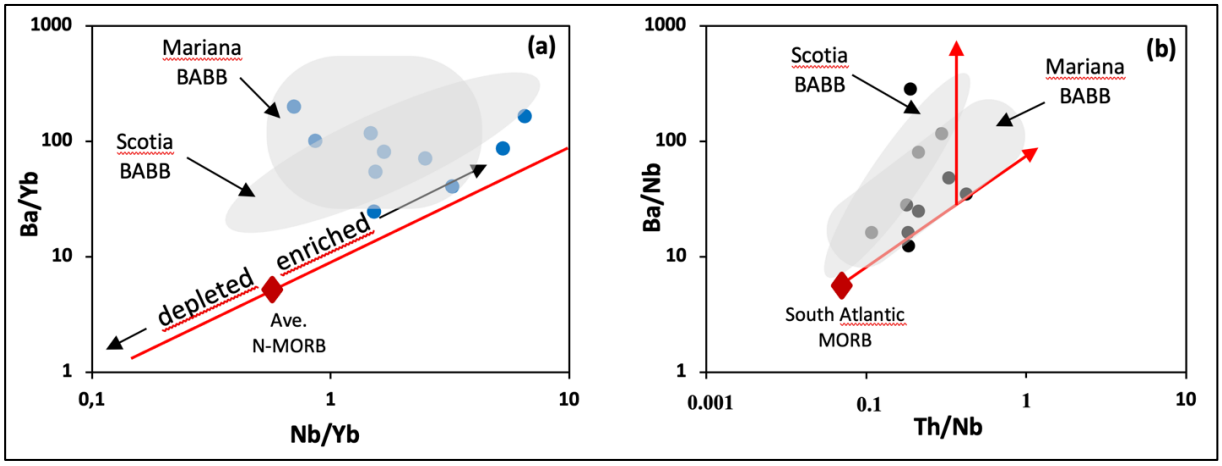


Fig. 12. a) Nb/Yb versus Ba/Yb diagram for spilitic basalts from the Chalky formation. Samples either cluster near the trend defined by subduction-unaffected MORB or are shifted toward higher Ba/Yb values; b) Th/Nb versus Ba/Nb diagram showing that most samples follow deep subduction trends, moving toward elevated Th/Nb ratios (adapted from Pearce and Stern, 2006)

The elemental ratios from the studied samples were compared with those of back-arc basin basalts (BABBs) from the western Pacific basins. As shown in figure 12a, BABBs exhibit higher Ba/Yb ratios than N-MORB, indicating a stronger influence of subducted barium in their mantle sources. Notably, the Ba/Yb ratios of the studied samples closely match those of the Mariana and Scotia BABBs. Based on this comparison, it is concluded that back-arc basin basalt (BABB) magmatism represents the dominant type in the studied samples.

Ba/Nb and Th/Nb ratios were used to evaluate the contributions of shallow and deep subduction in back-arc basins (Pearce and Stern, 2006), with Ba/Nb representing total subduction input and Th/Nb indicating deep subduction. In fig. 12b, most samples follow the deep-subduction trend toward higher Th/Nb values. Sample S8, however, deviates from this pattern, showing elevated Ba/Nb (283.13) and Ba/Yb (198.68) ratios, suggesting that its basaltic magma may have been contaminated by crustal material during ascent.

6. Conclusions

The Chalki basaltic rocks are interlayered with Pirispiki metasediments and are associated with multiple thrust sheets extending from Bitlis in southeastern Turkey to northern Iraq. These basaltic rocks from Chalki are spilitic basalts, predominantly composed of plagioclase, olivine, and pyroxene, exhibiting microporphyritic and amygdaloidal textures. According to the classification diagram, the studied spilitic basalts fall within the sub-alkaline basalt category. Tectonic discrimination diagrams indicate that these basalts mainly originated in a back-arc basin setting.

Trace element spider diagrams, comparing N-MORB and chondrite values, suggest a closer similarity to enriched E-MORB and ocean island basalts (OIB), reflecting a subduction-related geochemical signature. Consequently, these rocks likely formed from the partial melting of a spinel lherzolite source within a depleted mid-oceanic mantle. Sm-Nd isotopic data yield an age of 375 ±5.5 million years, interpreted as the time of intrusion and post-crystallization of the Chalki basalts. All analyzed samples show positive epsilon neodymium (εNd) values, indicating a mantle-derived origin with contributions from a depleted source and some crustal input. The timing of Chalki basaltic activity corresponds with the opening phases of the Proto-Tethys (Cambrian to Devonian) or Paleo-Tethys (mid-Silurian to Mesozoic) oceans. However, given the proximity of the Paleo-Tethys mid-ocean ridge

to northeastern Arabia, it is more likely that the Chalki volcanism is linked to the opening of the Paleo-Tethys Ocean.

Author contributions: CRediT

Ahmed M. Aqrawi: Conceptualization, Supervision, Writing – Original Draft, Writing, Review, and Editing.

Alan M. Koyi: Fieldwork methodology and validation; Data curation; Interpretation of petrological and field data; Writing, Review, and Editing.

Nihad M. Karo: Methodology design (geochemical/mineralogical); Formal analysis and interpretation of geochemical data; Validation; Resources; Writing, Review, and Editing.

Jolyana R. Petros: Lab work, maps preparation, tectonic interpretation, writing, review and Editing, Project Administration.

Declaration of Competing Interest

The authors declare that they have no competing financial interests or personal relationships that could influence the work reported in this study.

Acknowledgment

The authors express their gratitude to the technicians at the Geochemistry Laboratory, Washington State University (USA), for conducting the XRF and REE analyses. We also sincerely thank the staff of the Laboratory of Geochronological and Environmental Studies at the University of Brasília for their assistance with Nd and Sm isotope measurements. Special thanks are extended to Dr. Renas Koshnaw for his valuable scientific discussions and constructive comments, which greatly improved the manuscript.

Data Availability

All data generated or analyzed during this study are included in this published article.

7. ORCID

Ahmed M. Aqrawi: https://orcid.org/0000-0002-8754-0864

Alan M. Koyi: https://orcid.org/0000-0003-4375-0429

Nihad M. Karo: https://orcid.org/0000-0002-6976-9120

Jolyana R. Petros: https://orcid.org/0009-0000-8776-4465

References:

Akhtar, S., Saikia, A., Negi, P., Kalita, B.J., 2021. Back-arc basin origin for the basalts of the South Andaman Island Ophiolite (India). Episodes, 45, 5–27. https://doi.org/10.18814/epiiugs/2021/021001

Al-Hadidy, A.H., 2007. Paleozoic stratigraphic lexicon and hydrocarbon habitat of Iraq. GeoArabia, 12(3), 63–130.

Aldanmaz, E., Pearce, J.A., Thirlwall, M.F., Mitchell, J., 2000. Petrogenetic evolution of Late Cenozoic, post-collision volcanism in western Anatolia, Turkey. Journal of Volcanology and Geothermal Research, 102, 67–95. https://doi.org/10.1016/S0377-0273(00)00182-7

Ali, S.A., Omer, M.F., Aqrawi, A.M., 2016. Petrography, geochemistry, and provenance of the Chalki rocks in Kurdistan region, North Iraq. Arabian Journal of Geosciences, 9, 524. https://doi.org/10.1007/s12517-016-2545-0

Altinli, T.E., 1966. Geology of eastern and south-eastern Anatolia, Part II. Turkey Mineral Research and Exploration Institute Bulletin, 67, 1–22.

Aqrawi, A.A.M., Goff, J.C., Horbury, A.D., Sadooni, F.N., 2010. The Petroleum Geology of Iraq. Scientific Press, Beaconsfield, UK, 424 p.

Arndt, N.T., Lesher, C.M., Barnes, S.J., 2008. Komatiites. Cambridge University Press, Cambridge, 467.

Beydoun, Z.R., 1991. Arabian Plate Hydrocarbon Geology and Potential – A Plate Tectonic Approach. American Association of Petroleum Geologists Studies in Geology, 33. https://doi.org/10.1306/St33533

Brown, G.C., Thorpe, R.S., Webb, P.C., 1984. The geochemical characteristics of granitoids in contrasting arcs and comments on magma source. Journal of the Geological Society of London, 141, 413–426. https://doi.org/10.1144/gsjgs.141.3.0413

Buday, T., 1980. The Regional Geology of Iraq: Stratigraphy and Palaeogeography (Vol. 1). State Organization for Minerals, Directorate General for Geological Survey and Mineral Investigations, Baghdad.

Buday, T., Jassim, S.Z., 1987. The Regional Geology of Iraq: Tectonics, Magmatism, and Metamorphism (Vol. 2). State Organization for Minerals, Directorate General for Geological Survey and Mineral Investigations, Baghdad.

Çimen, O., Göncüoğlu, M.C., Sayıt, K., 2016. Geochemistry of the metavolcanic rocks from the Çangaldağ Complex in the Central Pontides: implications for the Middle Jurassic arc-back-arc system in the Neotethyan Intra-Pontide Ocean. Turkish Journal of Earth Sciences, 25, 491–512. https://doi.org/10.3906/yer-1603-11

Chin, E.J., Shimizu, K., Bybee, G.M., Erdman, M.E., 2018. On the development of the calc-alkaline and tholeiitic magma series: a deep crustal cumulate perspective. Earth and Planetary Science Letters, 482, 277–287. https://doi.org/10.1016/j.epsl.2017.11.016

Floyd, P.A., Kelling, G., Gökçen, S.L., Gökçen, S., 1991. Geochemistry and tectonic environment of basaltic rocks from the Misis ophiolitic mélange, south Turkey. Chemical Geology, 89, 263–280. https://doi.org/10.1016/0009-2541(91)90020-R

Gale, A., Dalton, C.A., Langmuir, C.H., Su, Y., Schilling, J.G., 2013. The mean composition of ocean ridge basalts. Geochemistry, Geophysics, Geosystems, 14, 489–518. https://doi.org/10.1029/2012GC004334

Jacobsen, S.B., Wasserburg, G.J., 1984. Sm-Nd isotopic evolution of chondrites and achondrites, II. Earth and Planetary Science Letters, 67, 137–150. https://doi.org/10.1016/0012-821X(84)90109-2

Jassim, S.Z., 2000. Regional Geology and Structural Timing of Tethys-Paleogeography and Hydrocarbon Systems. In: AAPG Cairo 2000 Conference on Ancient Oil-New Energy, Cairo (abstract).

Jiang, S.Y., Wang, R.C., Xu, X.S., Zhao, K.D., 2005. Mobility of high field strength elements (HFSE) in magmatic-, metamorphic-, and submarine-hydrothermal systems. Physics and Chemistry of the Earth, 30, 1020–1029. https://doi.org/10.1016/j.pce.2004.11.004

Jochum, K.P., Nohl, U., Herwig, K., Lammel, E., Stoll, B., Hofmann, A.W., 2007. GeoReM: a new geochemical database for reference materials and isotopic standards. Geostandards and Geoanalytical Research, 29(3), 333–338. https://doi.org/10.1111/j.1751-908X.2005.tb00904.x

Kettanah, Y.A., Abdulrahman, A.S., Ismail, S.A., MacDonald, D.J., Al Humadi, H., 2021. Petrography, mineralogy, and geochemistry of the Hemrin Basalt, Northern Iraq: implications for petrogenesis and geotectonics. Lithos, 390–391, 106109. https://doi.org/10.1016/j.lithos.2021.106109

Kettanah, Y.A., Bamarni, A.H., 2018. Petrogenesis, geochemistry and tectonic setting of a basaltic body within the Gercus Formation of northern Iraq: first record for Eocene anorogenic volcanic activity in the region. Turkish Journal of Earth Sciences, 27(6), 460–491. https://doi.org/10.3906/yer-1803-11

Kohn, B.P., Eyal, M., Feinstein, S., 1992. A major Late Devonian–Early Carboniferous (Hercynian) thermotectonic event at the NW margin of the Arabian–Nubian Shield: evidence from zircon fission track dating. Tectonics, 11, 1018–1027. https://doi.org/10.1029/92TC00636

Koshnaw, R.I., Horton, B.K., Stockli, D.F., Barber, D.E., Tamar-Agha, M.Y., Kendall, J.J., 2017. Neogene shortening and exhumation of the Zagros fold-thrust belt and foreland basin in the Kurdistan region of northern Iraq. Tectonophysics, 694, 332–355. https://doi.org/10.1016/j.tecto.2016.11.016

Koshnaw, R.I., Schlunegger, F., Stockli, D.F., 2021. Detrital zircon provenance record of the Zagros Mountain building from the Neotethys obduction to the Arabia–Eurasia collision, NW Zagros fold–thrust belt, Kurdistan region of Iraq. Solid Earth, 12, 2479–2501. https://doi.org/10.5194/se-12-2479-2021

McDonough, W.F., Sun, S.S., 1995. The composition of the Earth. Chemical Geology, 120(3–4), 223–253. https://doi.org/10.1016/0009-2541(94)00140-4

Mullen, E.D., 1983. MnO/TiO2/P2O5: a minor element discriminant for basaltic rocks of oceanic environments and its implications for petrogenesis. Earth and Planetary Science Letters, 62, 53–62. https://doi.org/10.1016/0012-821X(83)90070-5

Pearce, J.A., Gale, G.H., 1977. Identification of ore-deposition environment from trace-element geochemistry of associated igneous host rocks. In: Volcanic Processes in Ore Genesis. Geological Society, London, Special Publications, 7, 14–24. https://doi.org/10.1144/GSL.SP.1977.007.01.03

Pearce, J.A., Norry, M.J., 1979. Petrogenetic implications of Ti, Zr, Y, and Nb variations in volcanic rocks. Contributions to Mineralogy and Petrology, 69, 33–47. https://doi.org/10.1007/BF00375192

Pearce, J.A., 1983. Role of the sub-continental lithosphere in magma genesis at active continental margins. In: Hawkesworth, C.J., Norry, M.J. (Eds.), Continental Basalts and Mantle Xenoliths. Shiva Publishing, Cheshire, 230–249.

Pearce, J.A., Stern, R.J., 2006. Origin of back-arc basin magmas: trace element and isotope perspectives. In: Back-Arc Spreading Systems: Geological, Biological, Chemical, and Physical Interactions. Geophysical Monograph Series 166. American Geophysical Union, Washington, DC, 63–86. https://doi.org/10.1029/166GM06

Rollinson, H.R., 1993. Using Geochemical Data: Evaluation, Presentation, Interpretation. Longman, London. https://doi.org/10.4324/9781315845548

Ruban, D.A., Al-Husseini, M.I., Iwasaki, Y., 2007. Review of Middle East Paleozoic plate tectonics. GeoArabia, 12(3), 35–56. https://doi.org/10.2113/geoarabia120335

Sharland, P.R., Archer, R., Casey, D.M., Davies, R.B., Hall, S.H., Heward, A.P., Horbury, A.D., Simmons, M.D., 2001. Arabian Plate Sequence Stratigraphy. GeoArabia Special Publication 2. Gulf Petrolink, Bahrain, 371 p.

Shervais, J.W., 1982. Ti-V plots and the petrogenesis of modern ophiolitic lavas. Earth and Planetary Science Letters, 59, 101–118. https://doi.org/10.1016/0012-821X(82)90120-0

Sissakian, V.K., Fouad, S.F., 2015. Geological map of Iraq, scale 1:1,000,000, 4th edition, 2012. Iraqi Bulletin of Geology and Mining, 11(1), 9–16.

Stern, R.J., Ren, M., Ali, K., Förster, H.J., Al Safarjalani, A., Nasir, S., Romer, R.L., 2014. Early Carboniferous (~357 Ma) crust beneath northern Arabia: tales from Tell Thannoun (southern Syria). Earth and Planetary Science Letters, 393, 83–93. https://doi.org/10.1016/j.epsl.2014.02.043

Sun, S.S., McDonough, W.F., 1989. Chemical and isotopic systematics of oceanic basalts: implications for mantle composition and processes. In: Saunders, A.D., Norry, M.J. (Eds.), Magmatism in the Ocean Basins. Geological Society, London, Special Publications, 42, 313–345. https://doi.org/10.1144/gsl.sp.1989.042.01.19

Taylor, S.R., McLennan, S.M., 1995. The geochemical evolution of the continental crust. Reviews of Geophysics, 33(2), 241–265. https://doi.org/10.1029/95RG00262

Van Bellen, R.C., Dunnington, H.V., Wetzel, R., Morton, D.M., 1959. Lexique Stratigraphique International, Volume III: Asie, Fascicule 10a: Iraq. Centre National de la Recherche Scientifique, Paris, 333 p.

Whalen, J.B., Syme, E.C., Stern, R.A., 1999. Geochemical and Nd isotopic evolution of Paleoproterozoic arc-type granitoid magmatism in the Flin Flon Belt, Trans-Hudson Orogen, Canada. Canadian Journal of Earth Sciences, 36, 227–250. https://doi.org/10.1139/cjes-36-2-227

Wharton, M.R., Hathway, B., Colley, H., 1995. Volcanism associated with extension in an Oligocene-Miocene arc, southwestern Viti Levu, Fiji. In: Smellie, J.L. (Ed.), Volcanism Associated with Extension at Consuming Plate Margins. Geological Society, London, Special Publications, 81, 95–114. https://doi.org/10.1144/gsl.sp.1994.081.01.01

Winchester, J.A., Floyd, P.A., 1977. Geochemical discrimination of different magma series and their differentiation products using immobile elements. Chemical Geology, 20, 325–343. https://doi.org/10.1016/0009-2541(77)90057-2

Wood, B.J., Graham, C.M., 1986. Infiltration of aqueous fluid and high fluid:rock ratios during greenschist facies metamorphism. Journal of Petrology, 27(3), 751–761. https://doi.org/10.1093/petrology/27.3.751

Woodhead, J.D., 1988. The origin of geochemical variations in Mariana lavas: a general model for petrogenesis in intra-oceanic island arcs. Journal of Petrology, 29(4), 805–830. https://doi.org/10.1093/petrology/29.4.805

Woodhead, J.D., Eggins, S., Gamble, J., 1993. High field strength and transition element systematics in island arc and back-arc basin basalts: evidence for multi-phase melt extraction and a depleted mantle wedge. Earth and Planetary Science Letters, 114, 491–504. https://doi.org/10.1016/0012-821X(93)90078-N

Zebari, M., Balling, P., Grützner, C., Navabpour, P., Witte, J., Ustaszewski, K., 2020. Structural style of the NW Zagros Mountains and the role of basement thrusting for its Mountain Front Flexure, Kurdistan Region of Iraq. Journal of Structural Geology, 141, 104206. https://doi.org/10.1016/j.jsg.2020.104206